

**Supporting figures and tables
for
*Radiative effects of inter-annually varying versus
inter-annually invariant aerosol emissions from fires***

Benjamin S. Grandey^{*1}, Hsiang-He Lee¹, and Chien Wang^{1,2}

¹Center for Environmental Sensing and Modeling, Singapore-MIT Alliance for Research
and Technology, Singapore.

²Center for Global Change Science, Massachusetts Institute of Technology, Cambridge,
Massachusetts, USA.

July 8, 2016

^{*}benjamin@smart.mit.edu

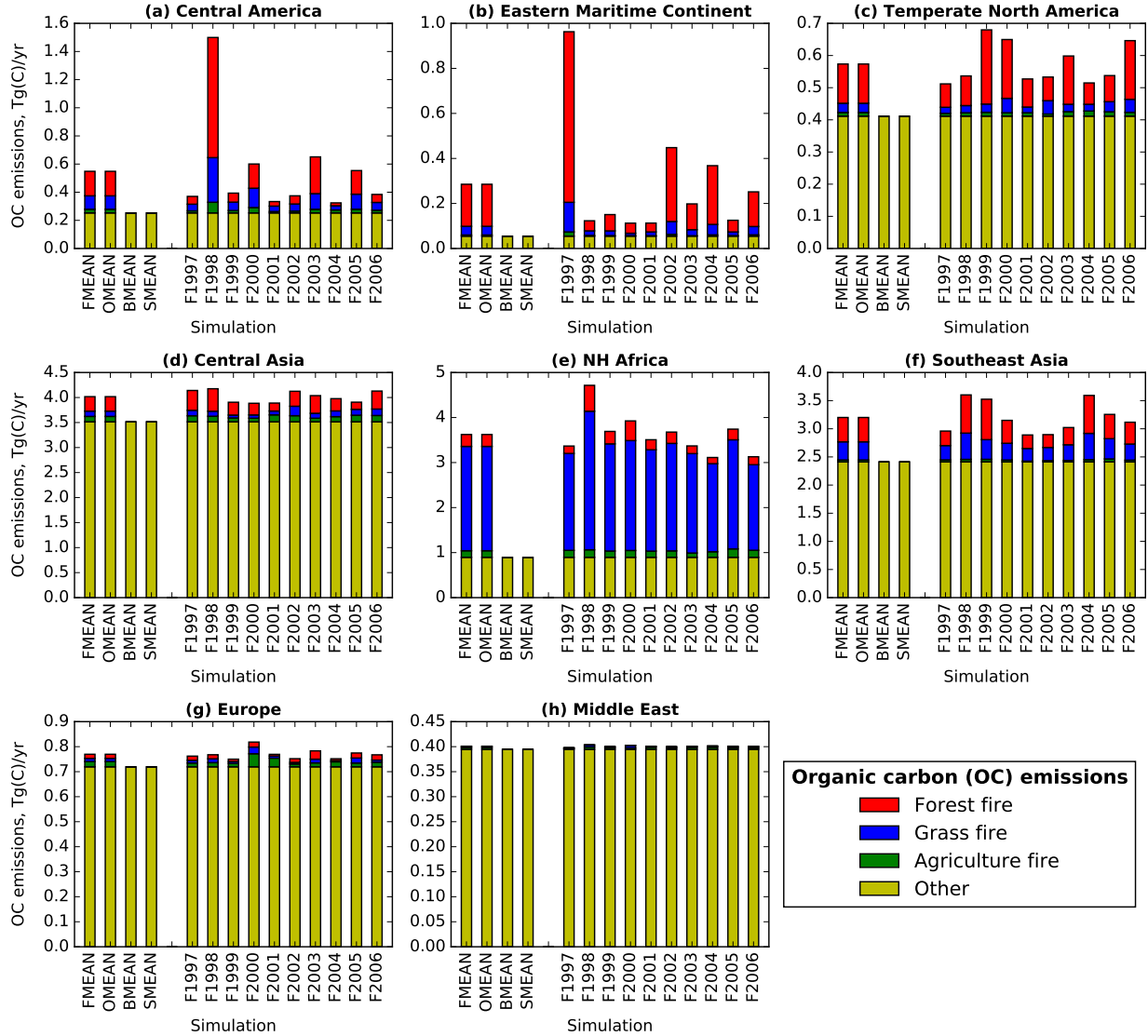


Figure S1: Organic carbon (OC) annual emissions for eight regions. Emissions for the globe and seven other regions are shown in Fig. 2 of the main manuscript.

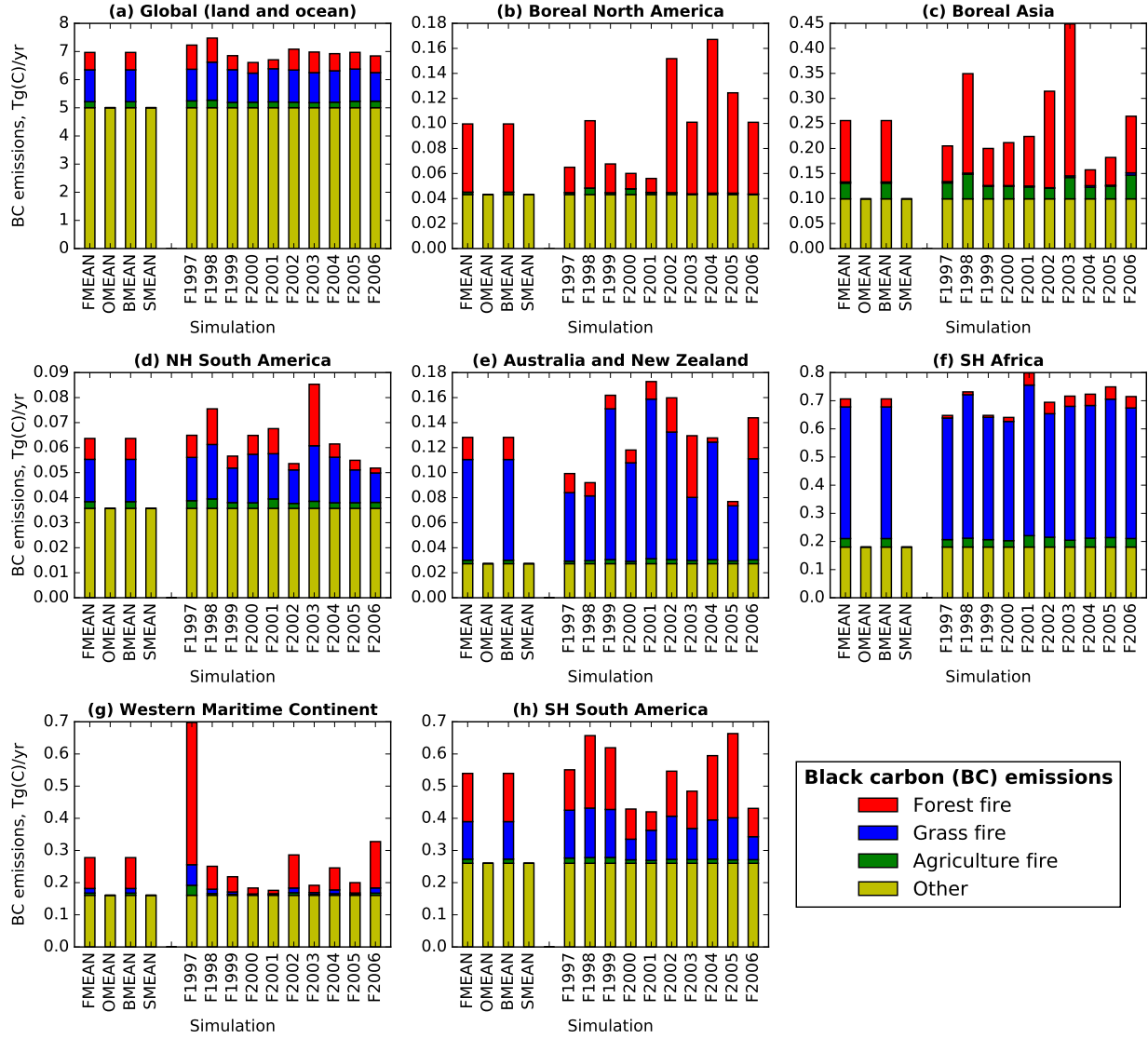


Figure S2: Black carbon (BC) annual emissions for (a) the globe and (b)–(h) seven regions. Emissions for another eight regions are shown in Fig. S3.

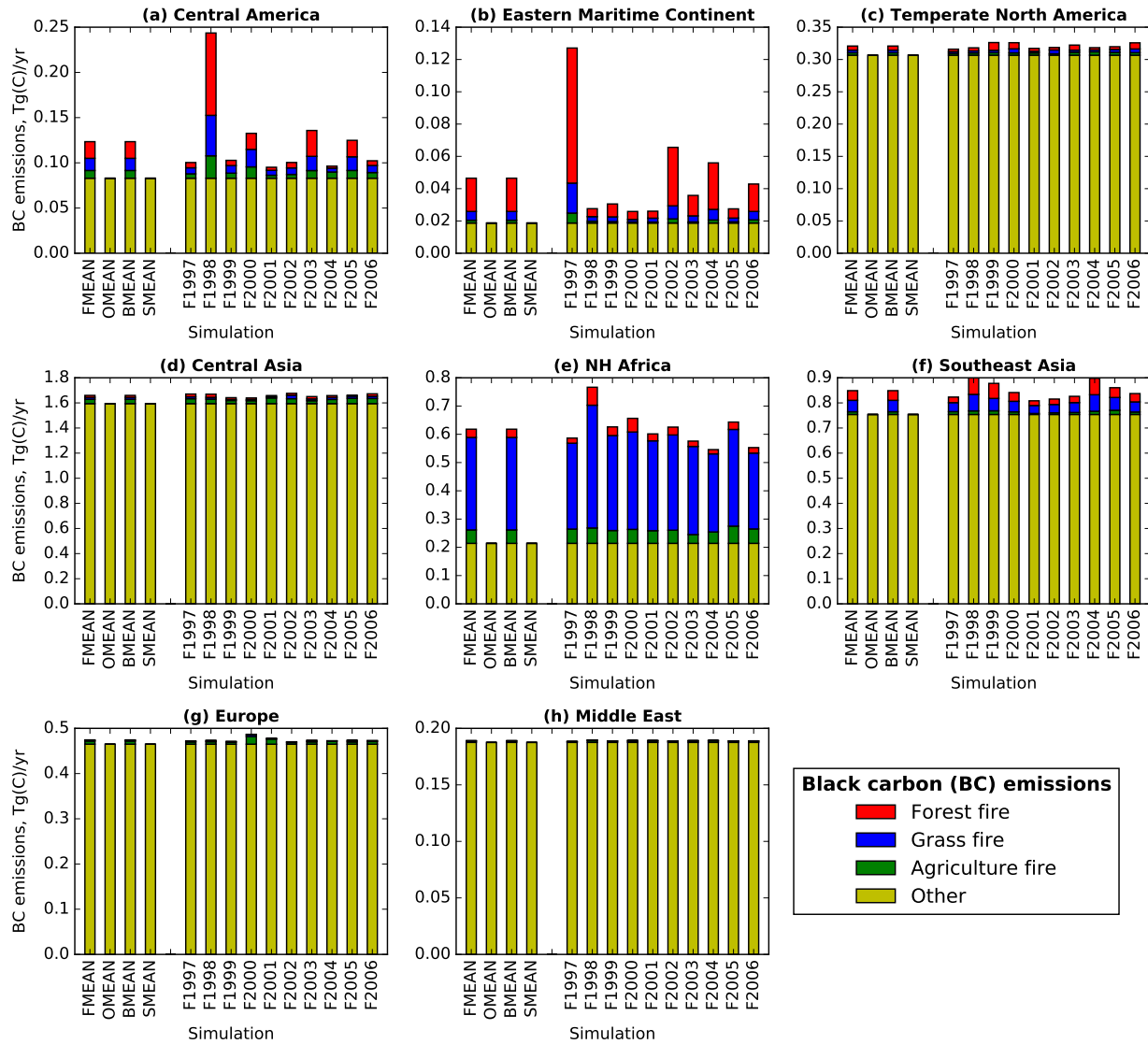


Figure S3: Black carbon (BC) annual emissions for eight regions. Emissions for the globe and seven other regions are shown in Fig. S2.

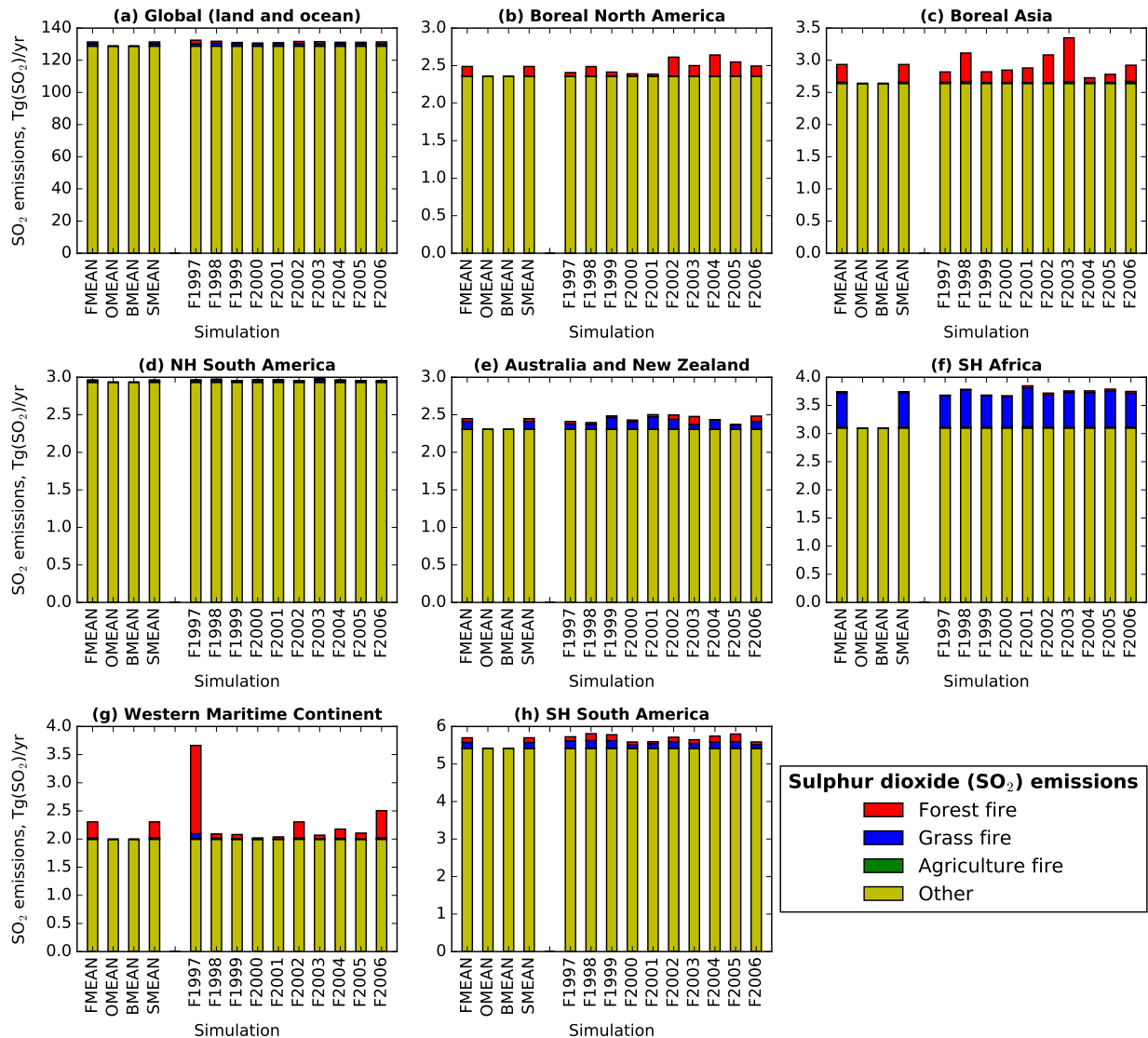


Figure S4: Sulphur dioxide (SO_2) annual emissions for (a) the globe and (b)–(h) seven regions. In the simulations, 2.5% of these SO_2 emissions are emitted as primary sulphate. Emissions for another eight regions are shown in Fig. S5.

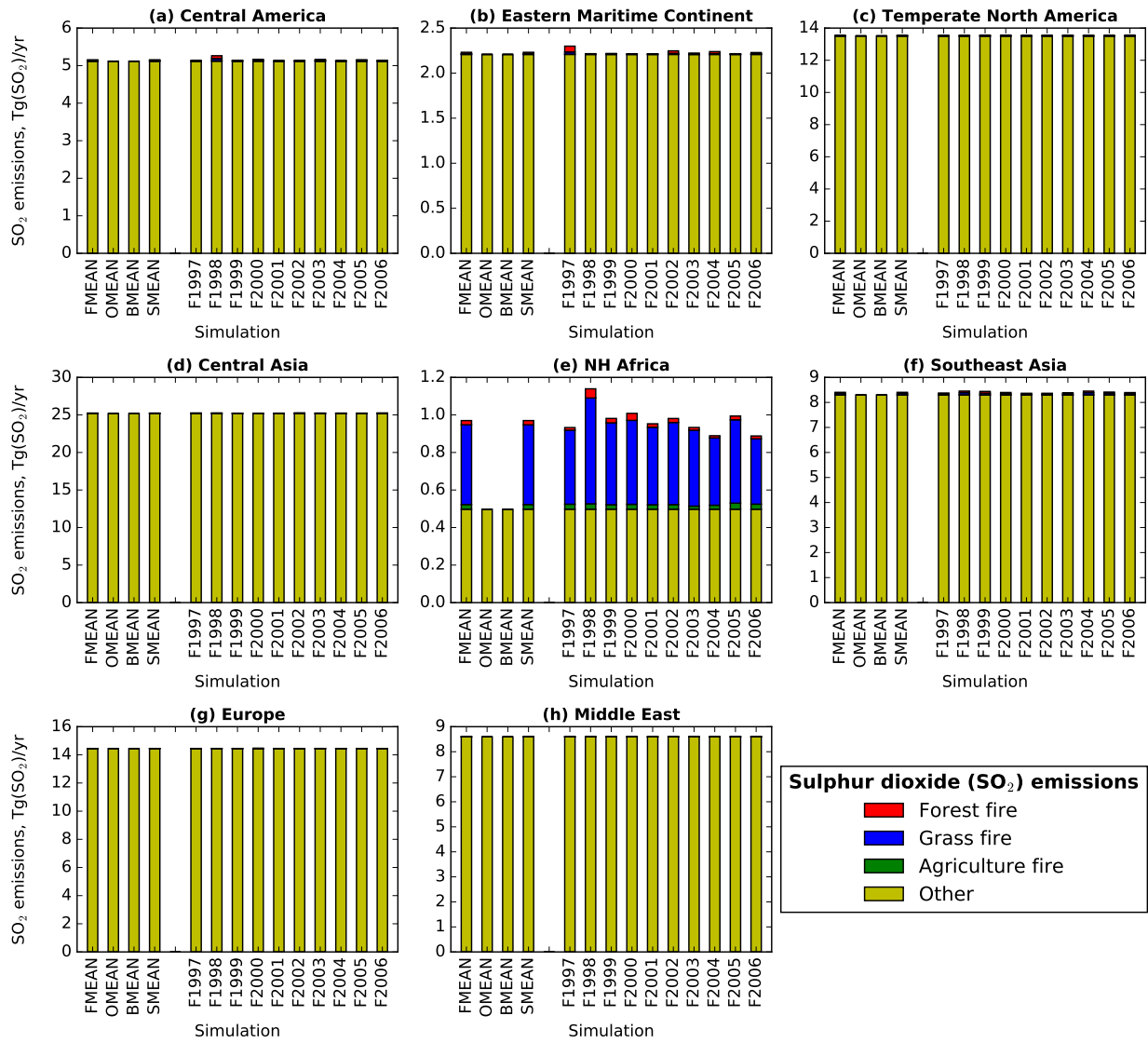


Figure S5: Sulphur dioxide (SO_2) annual emissions for eight regions. In the simulations, 2.5% of these SO_2 emissions are emitted as primary sulphate. Emissions for the globe and seven other regions are shown in Fig. S4.

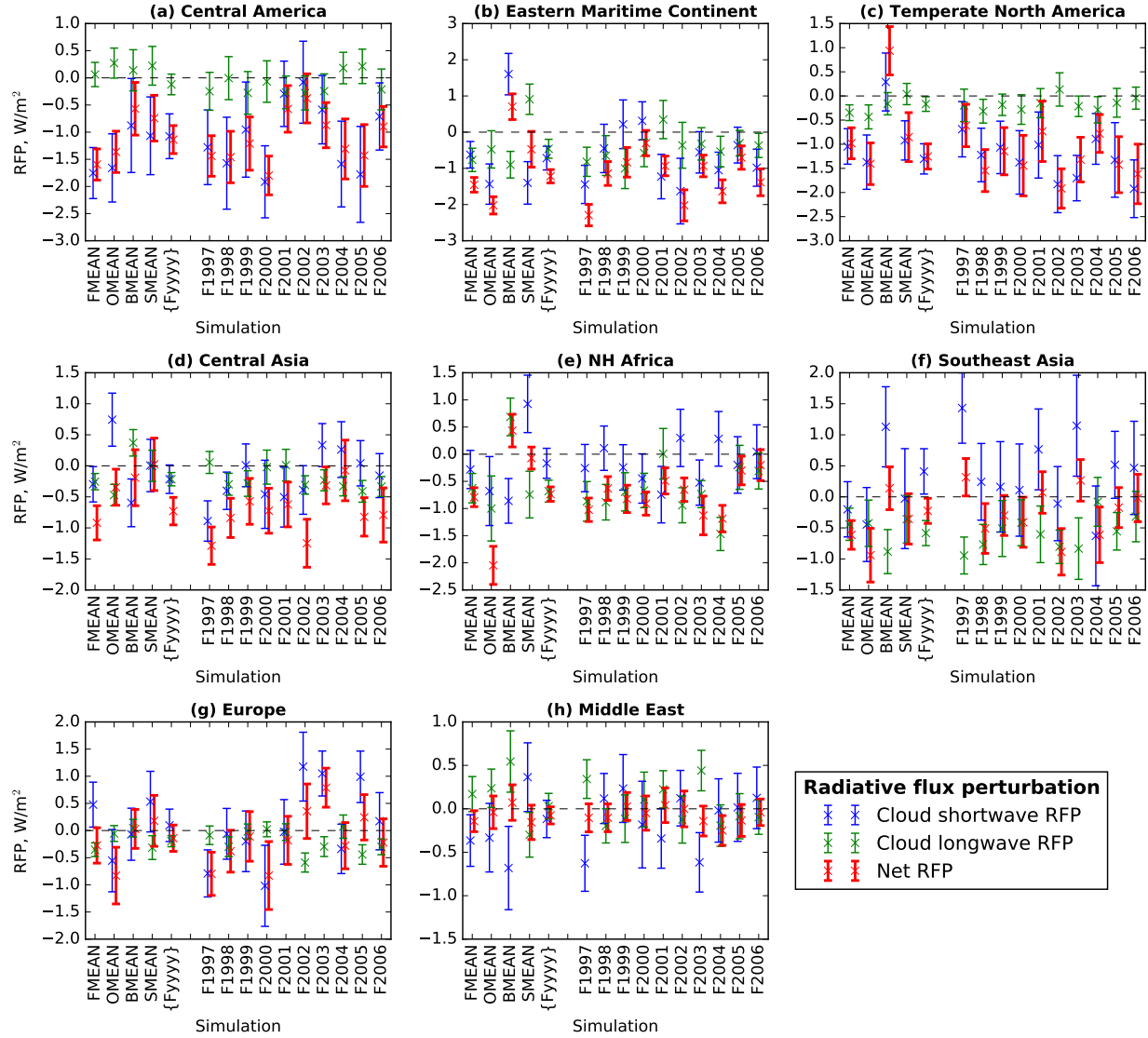


Figure S6: Cloud shortwave, cloud longwave, and net (all components, shortwave plus longwave) top-of-atmosphere radiative flux perturbations (RFPs) for eight regions. The RFPs are relative to simulation F0. Error bars represent combined standard error – e.g. for the F1997 net RFP error bars, the combined standard error equals $\sqrt{\frac{s_{F0}^2}{N_{F0}} + \frac{s_{F1997}^2}{N_{F1997}}}$, where s_{F0} and s_{F1997} are the corrected sample standard deviations, and $N_{F0} = 42$ and $N_{F1997} = 12$ are the sample sizes. Results for the globe and seven other regions are shown in Fig. 3 of the main manuscript.

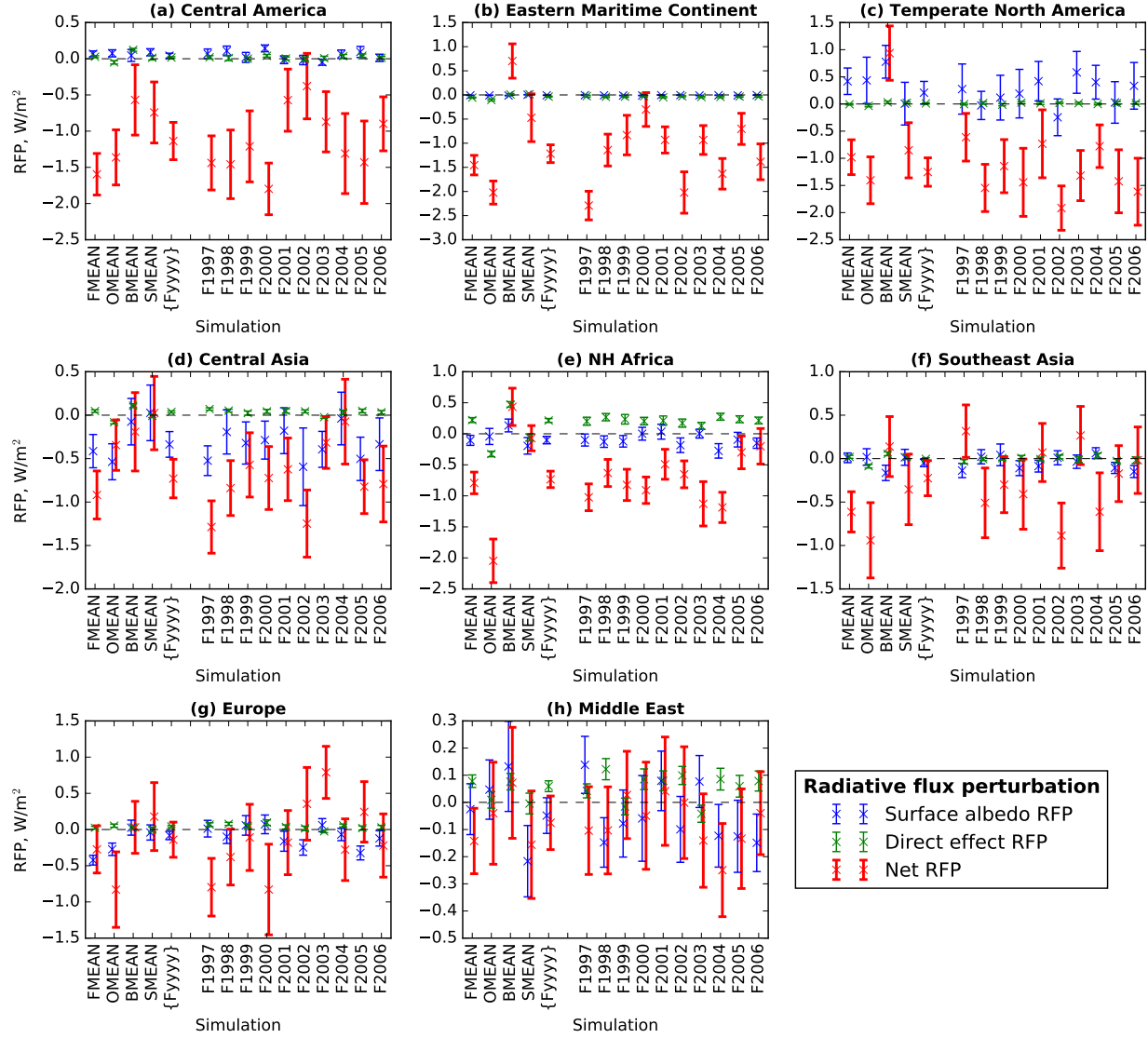


Figure S7: Surface albedo, aerosol direct effect, and net (all components, shortwave plus longwave) top-of-atmosphere radiative flux perturbations (RFPs) for eight regions. The RFPs are relative to simulation F0. Error bars represent combined standard error. Results for the globe and seven other regions are shown in Fig. 4 of the main manuscript.

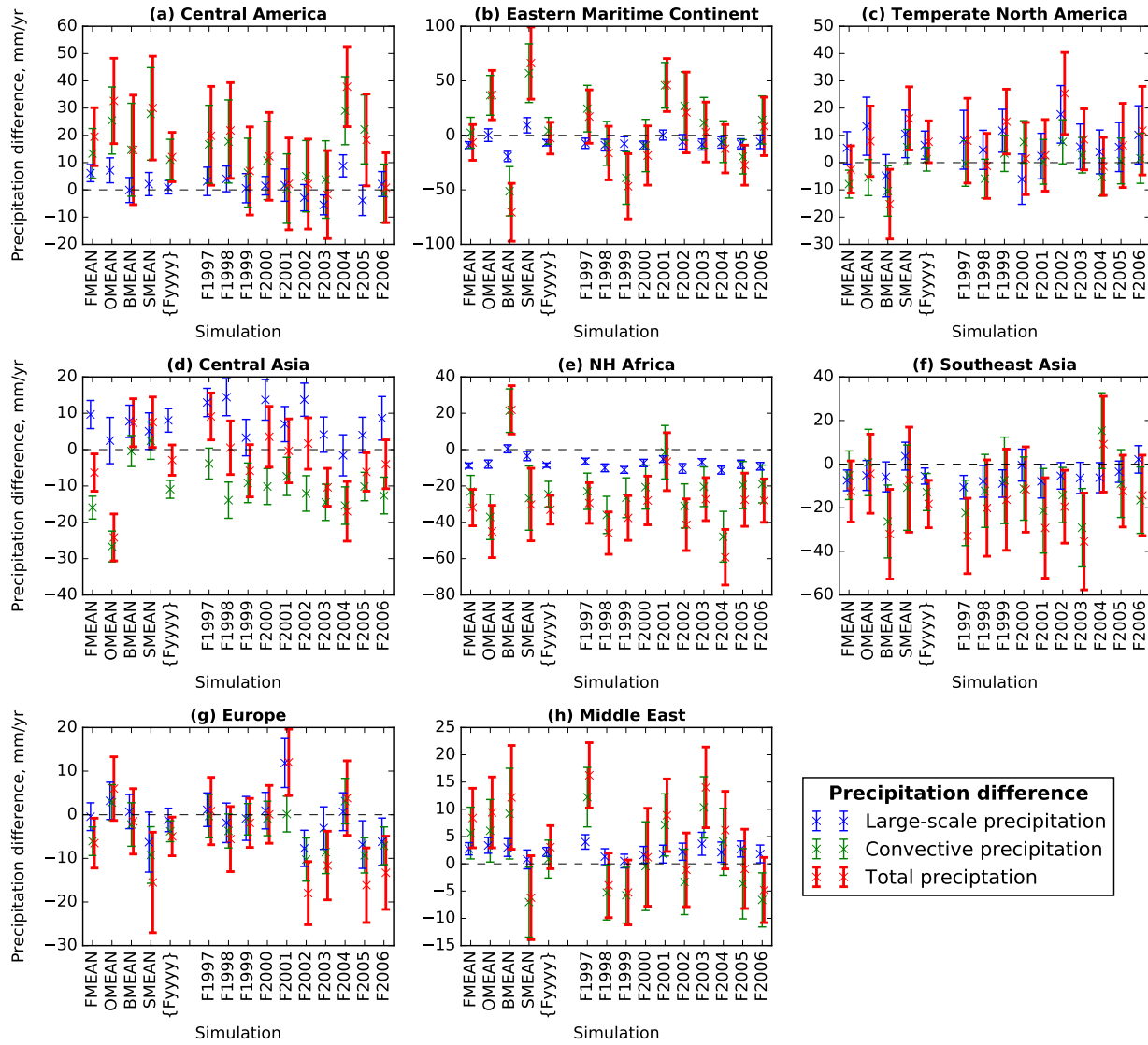


Figure S8: Large-scale, convective, and total (large-scale plus convective) annual precipitation differences, relative to simulation F0, for eight regions. Error bars represent combined standard error. Results for the globe and seven other regions are shown in Fig. 7 of the main manuscript.

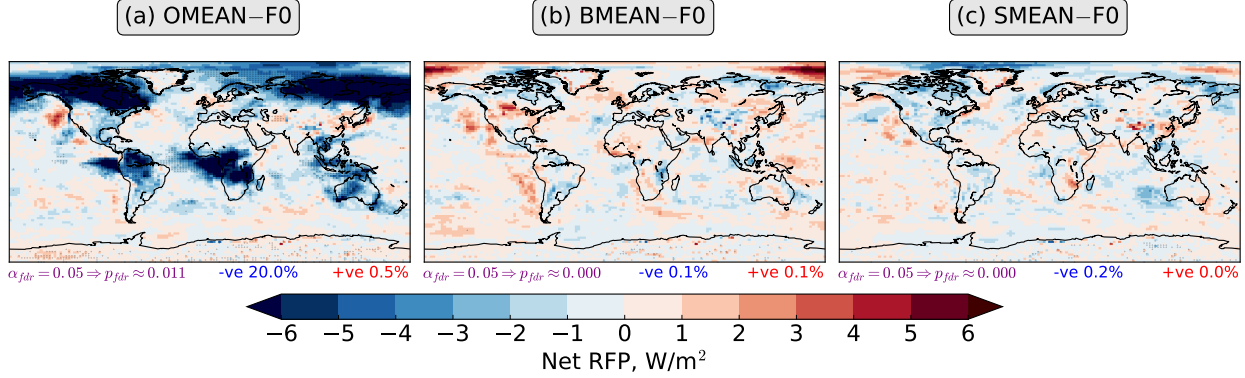


Figure S9: Net (shortwave plus longwave) top-of-atmosphere radiative flux perturbations (RFPs), relative to simulation F0, for simulations (a) OMEAN, (b) BMEAN, and (c) SMEAN. Stippling indicates differences that are statistically significant at a significance level of $\alpha_{fdr} = 0.05$ after controlling the False Discovery Rate (FDR; Benjamini and Hochberg, 1995; Wilks, 2016). The two-tailed p -values are generated by Welch's t -test, using annual mean data as the input. The approximate p -value threshold, p_{fdr} , is written in purple underneath each map. The percentage of the globe (area-weighted) over which negative ("–ve") statistically significant differences occur is written in blue text underneath each map, while the percentage of the globe over which positive ("+ve") statistically significant differences occur is written in red text.

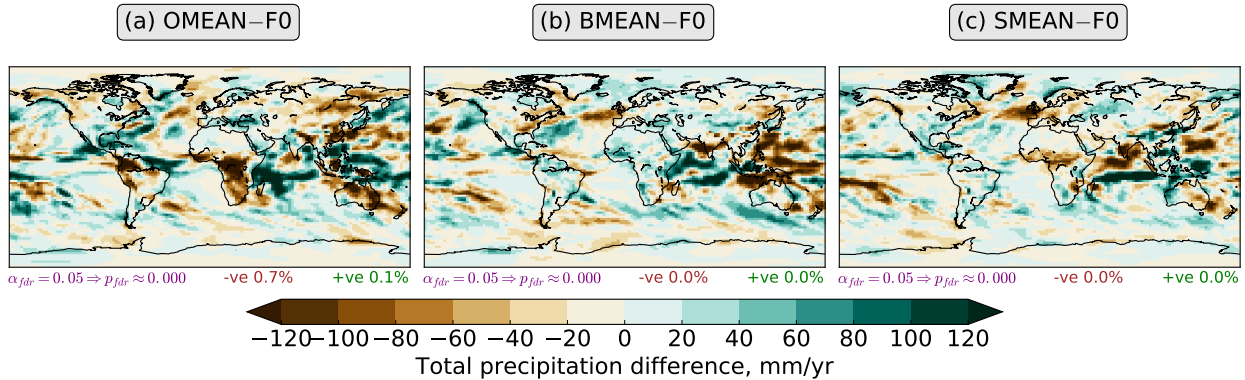
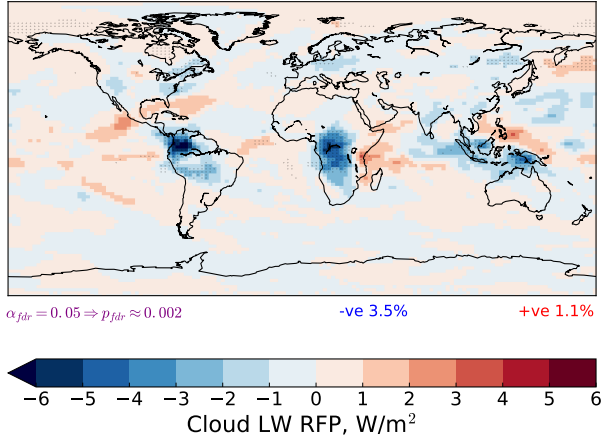
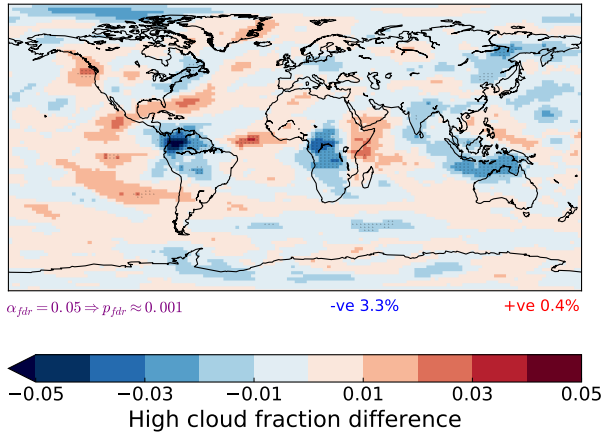


Figure S10: Total (convective plus large-scale) annual precipitation differences, relative to simulation F0, for simulations (a) OMEAN, (b) BMEAN, and (c) SMEAN. Stippling indicates differences that are statistically significant at a significance level of $\alpha_{fdr} = 0.05$ after controlling the False Discovery Rate (FDR; Benjamini and Hochberg, 1995; Wilks, 2016). The two-tailed p -values are generated by Welch's t -test, using annual mean data as the input. The approximate p -value threshold, p_{fdr} , is written in purple underneath each map. The percentage of the globe (area-weighted) over which negative ("–ve") statistically significant differences occur is written in brown text underneath each map, while the percentage of the globe over which positive ("+ve") statistically significant differences occur is written in green text.

(a) Cloud LW RFP; FMEAN–F0



(b) High cloud fraction; FMEAN–F0



(c) Ice water path; FMEAN–F0

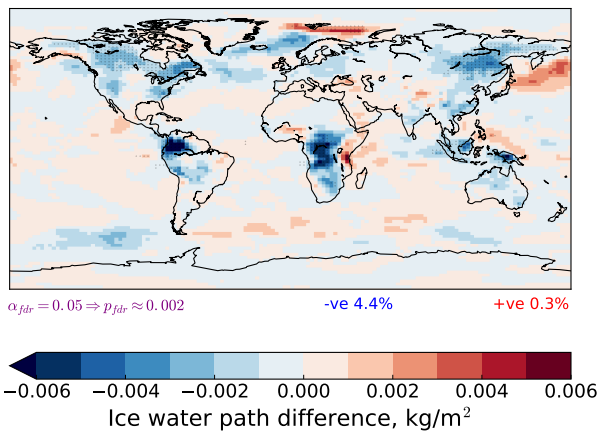


Figure S11: (a) Cloud longwave (LW) top-of-atmosphere radiative flux perturbations (RFPs), (b) high cloud fraction differences, and (c) grid-box-average ice water path differences for simulation FMEAN relative to simulation F0. Stippling indicates differences that are statistically significant at a significance level of $\alpha_{fdr} = 0.05$ after controlling the False Discovery Rate (FDR; Benjamini and Hochberg, 1995; Wilks, 2016). The two-tailed p -values are generated by Welch's t -test, using annual mean data as the input. The approximate p -value threshold, p_{fdr} , is written in purple underneath each map. The percentage of the globe (area-weighted) over which negative ("–ve") statistically significant differences occur is written in blue text underneath each map, while the percentage of the globe over which positive ("+ve") statistically significant differences occur is written in red text.

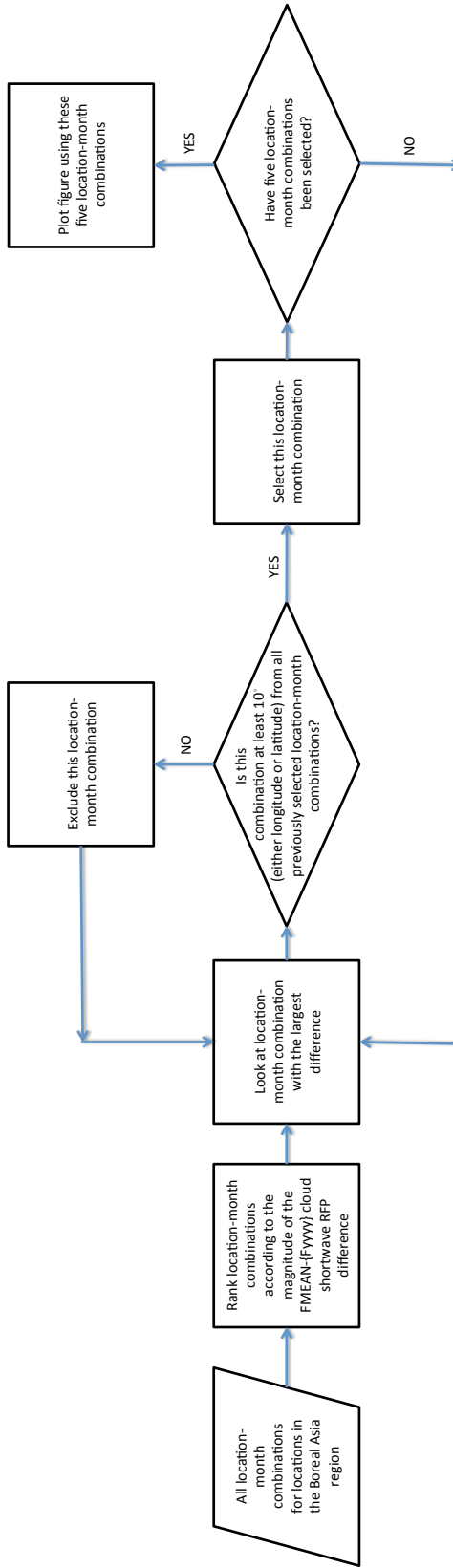


Figure S12. Flowchart showing the method of selection for the five location-month combinations shown in Fig. 9 of the main manuscript. Three criteria have been specified for the selection process: (1) within the Boreal Asia region, select the location-month combinations with (2) the largest FMEAN- $\{F_{yyyy}\}$ cloud shortwave RFP differences, (3) at least 10° (either longitude or latitude) from one another. The available locations are constrained by the horizontal resolution of approximately $1.9^\circ \times 2.5^\circ$.

Table S1: Cloud longwave top-of-atmosphere radiative flux perturbation (RFP) differences for different simulation combinations and regions. Combined standard errors have been calculated using corrected sample standard deviations – e.g. the standard error for the global $\{F_{yyyy}\}$ –F0 difference was calculated using $\sqrt{\frac{s_{\{F_{yyyy}\}}^2}{N_{\{F_{yyyy}\}}} + \frac{s_{F0}^2}{N_{F0}}}$, where $s_{\{F_{yyyy}\}}$ and s_{F0} are the corrected sample standard deviations, and $N_{\{F_{yyyy}\}} = 120$ and $N_{F0} = 42$ are the sample sizes. Significance has been tested using Welch’s t -test: ‘*’ indicates differences that are statistically significant at two-tailed $p < 0.05$; and ‘**’ indicates differences that are statistically significant at two-tailed $p < 0.01$.

Region	Cloud longwave radiative flux perturbation (RFP), W m^{-2}		
	FMEAN–F0	$\{F_{yyyy}\}$ –F0	FMEAN– $\{F_{yyyy}\}$
	“conventional”	“revised”	difference
Global (land and ocean)	$-0.11 \pm 0.02^{**}$	$-0.13 \pm 0.02^{**}$	$+0.01 \pm 0.02$
Boreal North America	-0.10 ± 0.08	-0.12 ± 0.07	$+0.02 \pm 0.06$
Boreal Asia	$-0.24 \pm 0.10^{*}$	$-0.23 \pm 0.08^{**}$	-0.01 ± 0.09
NH South America	$-2.65 \pm 0.36^{**}$	$-2.43 \pm 0.30^{**}$	-0.22 ± 0.29
Australia and New Zealand	-0.24 ± 0.20	$-0.44 \pm 0.16^{**}$	$+0.20 \pm 0.18$
SH Africa	$-1.35 \pm 0.22^{**}$	$-1.44 \pm 0.18^{**}$	$+0.09 \pm 0.18$
Western Maritime Continent	$-1.74 \pm 0.34^{**}$	$-1.55 \pm 0.29^{**}$	-0.19 ± 0.27
SH South America	$-0.85 \pm 0.14^{**}$	$-0.76 \pm 0.11^{**}$	-0.08 ± 0.11
Central America	$+0.06 \pm 0.22$	-0.12 ± 0.19	$+0.18 \pm 0.18$
Eastern Maritime Continent	$-0.77 \pm 0.32^{*}$	-0.46 ± 0.26	-0.31 ± 0.26
Temperate North America	$-0.35 \pm 0.16^{*}$	-0.17 ± 0.15	-0.18 ± 0.12
Central Asia	-0.25 ± 0.13	$-0.22 \pm 0.11^{*}$	-0.04 ± 0.11
NH Africa	$-0.63 \pm 0.27^{*}$	$-0.68 \pm 0.20^{**}$	$+0.05 \pm 0.23$
Southeast Asia	-0.44 ± 0.26	$-0.58 \pm 0.20^{**}$	$+0.14 \pm 0.22$
Europe	$-0.35 \pm 0.13^{**}$	-0.20 ± 0.10	-0.16 ± 0.10
Middle East	$+0.17 \pm 0.20$	$+0.03 \pm 0.15$	$+0.14 \pm 0.17$

Table S2: Surface albedo effect top-of-atmosphere radiative flux perturbation (RFP) differences for different simulation combinations and regions. The surface albedo RFP includes “both changes in snow albedo due to deposition of absorbing aerosol, and changes in snow cover induced by deposition and by the other aerosol forcing mechanisms” (Ghan, 2013). Combined standard errors have been calculated. Significance has been tested using Welch’s *t*-test: ‘*’ indicates differences that are statistically significant at two-tailed $p < 0.05$; and ‘**’ indicates differences that are statistically significant at two-tailed $p < 0.01$.

Region	Surface albedo radiative flux perturbation (RFP), W m^{-2}		
	FMEAN–F0	$\{\text{Fyyyy}\} - \text{F0}$	FMEAN– $\{\text{Fyyyy}\}$
	“conventional”	“revised”	difference
Global (land and ocean)	$-0.08 \pm 0.02^{**}$	$-0.07 \pm 0.01^{**}$	-0.01 ± 0.02
Boreal North America	$-0.57 \pm 0.19^{**}$	$-0.42 \pm 0.15^{**}$	-0.15 ± 0.16
Boreal Asia	-0.26 ± 0.24	-0.22 ± 0.18	-0.04 ± 0.19
NH South America	$-0.03 \pm 0.01^{**}$	$-0.02 \pm 0.01^{**}$	-0.01 ± 0.01
Australia and New Zealand	-0.13 ± 0.08	$-0.18 \pm 0.06^{**}$	$+0.05 \pm 0.07$
SH Africa	$-0.07 \pm 0.03^*$	$-0.09 \pm 0.03^{**}$	$+0.02 \pm 0.03$
Western Maritime Continent	$-0.01 \pm 0.00^{**}$	$-0.01 \pm 0.00^{**}$	$+0.00 \pm 0.00$
SH South America	$-0.03 \pm 0.01^*$	$-0.04 \pm 0.01^{**}$	$+0.01 \pm 0.01$
Central America	$+0.07 \pm 0.04$	$+0.04 \pm 0.03$	$+0.03 \pm 0.03$
Eastern Maritime Continent	$-0.01 \pm 0.00^{**}$	$-0.01 \pm 0.00^{**}$	-0.00 ± 0.00
Temperate North America	$+0.42 \pm 0.24$	$+0.21 \pm 0.21$	$+0.21 \pm 0.20$
Central Asia	$-0.41 \pm 0.19^*$	$-0.34 \pm 0.15^*$	-0.08 ± 0.16
NH Africa	-0.11 ± 0.08	-0.10 ± 0.06	-0.00 ± 0.07
Southeast Asia	$+0.01 \pm 0.06$	-0.05 ± 0.04	$+0.06 \pm 0.05$
Europe	$-0.42 \pm 0.07^{**}$	-0.08 ± 0.06	$-0.34 \pm 0.06^{**}$
Middle East	-0.03 ± 0.09	-0.05 ± 0.07	$+0.02 \pm 0.08$

Table S3: Direct effect top-of-atmosphere radiative flux perturbation (RFP) differences for different simulation combinations and regions. Combined standard errors have been calculated. Significance has been tested using Welch's *t*-test: '*' indicates differences that are statistically significant at two-tailed $p < 0.05$; and '**' indicates differences that are statistically significant at two-tailed $p < 0.01$.

Region	Direct effect radiative flux perturbation (RFP), W m^{-2}		
	FMEAN–F0	$\{\text{Fyyyy}\}–\text{F0}$	FMEAN– $\{\text{Fyyyy}\}$
	“conventional”	“revised”	difference
Global (land and ocean)	+0.04 ± 0.00**	+0.04 ± 0.00**	-0.00 ± 0.00
Boreal North America	+0.03 ± 0.00**	+0.02 ± 0.00**	+0.01 ± 0.00
Boreal Asia	+0.04 ± 0.01**	+0.01 ± 0.01*	+0.02 ± 0.01**
NH South America	-0.07 ± 0.02**	-0.06 ± 0.02**	-0.01 ± 0.02
Australia and New Zealand	-0.01 ± 0.02	-0.04 ± 0.01*	+0.02 ± 0.02
SH Africa	+0.14 ± 0.01**	+0.14 ± 0.01**	-0.00 ± 0.01
Western Maritime Continent	-0.09 ± 0.01**	-0.08 ± 0.01**	-0.01 ± 0.01
SH South America	-0.08 ± 0.01**	-0.07 ± 0.01**	-0.01 ± 0.01
Central America	+0.03 ± 0.01	+0.02 ± 0.01	+0.01 ± 0.01
Eastern Maritime Continent	-0.06 ± 0.01**	-0.03 ± 0.01**	-0.02 ± 0.01*
Temperate North America	-0.01 ± 0.01	+0.01 ± 0.01	-0.02 ± 0.01
Central Asia	+0.05 ± 0.01**	+0.04 ± 0.01**	+0.01 ± 0.01
NH Africa	+0.22 ± 0.04**	+0.21 ± 0.03**	+0.01 ± 0.03
Southeast Asia	+0.02 ± 0.02	-0.00 ± 0.01	+0.02 ± 0.01
Europe	+0.02 ± 0.02	+0.04 ± 0.01**	-0.02 ± 0.02
Middle East	+0.08 ± 0.02**	+0.06 ± 0.02**	+0.02 ± 0.02

Table S4: Organic carbon (OC) concentration at the surface for different simulation combinations and regions. Standard errors have been calculated for the FMEAN and $\{F_{yyyy}\}$ values, while combined standard errors have been calculated for the FMEAN– $\{F_{yyyy}\}$ differences. For the FMEAN– $\{F_{yyyy}\}$ differences, significance has been tested using Welch’s *t*-test. None of the differences are statistically significant at two-tailed $p < 0.05$.

Region	Surface organic carbon (OC) concentration, ppbm ($= 10^{-9} \text{ kg kg}^{-1}$)		
	FMEAN	$\{F_{yyyy}\}$	FMEAN– $\{F_{yyyy}\}$
	“conventional”	“revised”	difference
Global (land and ocean)	0.368 ± 0.000	0.372 ± 0.003	-0.004 ± 0.003
Boreal North America	0.271 ± 0.001	0.285 ± 0.016	-0.013 ± 0.016
Boreal Asia	0.556 ± 0.003	0.573 ± 0.023	-0.018 ± 0.023
NH South America	0.446 ± 0.002	0.445 ± 0.008	0.001 ± 0.008
Australia and New Zealand	0.408 ± 0.002	0.413 ± 0.011	-0.005 ± 0.012
SH Africa	2.401 ± 0.007	2.403 ± 0.019	-0.002 ± 0.020
Western Maritime Continent	1.716 ± 0.012	1.840 ± 0.196	-0.124 ± 0.196
SH South America	1.058 ± 0.003	1.061 ± 0.026	-0.003 ± 0.026
Central America	0.657 ± 0.002	0.660 ± 0.029	-0.004 ± 0.029
Eastern Maritime Continent	0.195 ± 0.001	0.198 ± 0.012	-0.003 ± 0.012
Temperate North America	0.453 ± 0.002	0.456 ± 0.004	-0.003 ± 0.005
Central Asia	1.376 ± 0.004	1.386 ± 0.008	-0.010 ± 0.009
NH Africa	1.722 ± 0.006	1.722 ± 0.014	0.000 ± 0.015
Southeast Asia	2.552 ± 0.008	2.567 ± 0.012	-0.014 ± 0.015
Europe	0.505 ± 0.004	0.508 ± 0.003	-0.003 ± 0.005
Middle East	0.419 ± 0.001	0.420 ± 0.001	-0.001 ± 0.002

References

- Benjamini, Y. and Hochberg, Y.: Controlling the False Discovery Rate: A Practical and Powerful Approach to Multiple Testing, *J. R. Statist. Soc. B*, 57, 289–300, 1995.
- Ghan, S. J.: Technical Note: Estimating aerosol effects on cloud radiative forcing, *Atmospheric Chemistry and Physics*, 13, 9971–9974, doi:10.5194/acp-13-9971-2013, 2013.
- Wilks, D.: The stippling shows statistically significant gridpoints: How Research Results are Routinely Overstated and Over-interpreted, and What to Do About It, *Bulletin of the American Meteorological Society*, doi:10.1175/BAMS-D-15-00267.1, 2016.